arXiv:1211.0150v1 [cond-mat.mes-hall] 1 Nov 2012

,

Semiclassical Klein Tunneling with Berry Phase Corrections in Graphene

Christoph M. Puetter,[1, 2, *] Satoru Konabe,[2, 3] Yasuhiro Hatsugai,[2, 3, 4] and Kenji Shiraishi[1, 2, 3]
[1] *Center for Computational Sciences, University of Tsukuba, 1-1-1 Tennodai, Tsukuba, 305-8577, Japan*
[2] *CREST, Japan Science and Technology Agency, 4-1-8 Honcho Kawaguchi, 332-0012, Japan*
[3] *Graduate School of Pure and Applied Sciences, University of Tsukuba, 1-1-1 Tennodai, Tsukuba, 305-8577, Japan*
[4] *Center for Interdisciplinary Research, Tohoku University, Sendai 980-8578, Japan*

We study the transport dynamics of semiclassical electrons in graphene in the Klein tunneling regime by scattering wave packets off a potential step while taking the full graphene Hamiltonian into account. Besides establishing the basic transmission characteristics for zigzag and armchair step edges, our numerical simulation suggests that the wave packet dynamics is substantially affected by the Berry curvature, which induces lateral shifts near the step edge reminiscent of the Hall effect of light. This anomalous correction can be relevant for recent Klein tunneling experiments.

PACS numbers: 72.80.Vp

Introduction — Graphene possesses extraordinary electronic transport properties due to the two special points in the band structure where conduction and valence band meet. At these so-called Dirac points the energy dispersion is conical, and electrons circling around each Dirac point acquire a nontrivial Berry phase of $\pm\pi$ [1]. Such a nontrivial Berry phase can lead to remarkable transport phenomena as displayed by the half-integer quantum Hall effect in graphene [2–4] and the intrinsic anomalous Hall effect in ferromagnetic materials [5]. The Klein paradox, too, is closely associated with the conical Dirac dispersion and may just as well be affected by a nontrivial band topology. The Klein paradox refers to the almost certain transmission of relativistic Dirac fermions across a potential barrier regardless of its height and width [6]. Considerable effort has recently been put into observing and exploring the Klein phenomenon in graphene devices [7–13], with evidence recently reported in [10] based on resistance measurements across a potential barrier and comparison with theoretical predictions for ballistic and diffusive transport. The authors, however, also pointed out unresolved discrepancies with the expected angle dependence of Klein tunneling.

Theoretical treatments of Klein tunneling in graphene usually rely on single valley linearized Dirac bands and plane wave approaches [14–17]. A semiclassical wave packet approach, however, can give further insight into the effective dynamics of Bloch electrons in bands with nontrivial topologies [18, 19]. This is evident from the semiclassical equations of motion for Bloch electrons

$$\dot{\mathbf{r}} = \nabla_{\mathbf{k}}\epsilon_{\mathbf{k}} - \dot{\mathbf{k}} \times \mathbf{\Omega}_{\mathbf{k}}, \qquad \dot{\mathbf{k}} = -e(\mathbf{E} + \dot{\mathbf{r}} \times \mathbf{B}), \tag{1}$$

where $\mathbf{r}$ stands for the electron position, $\epsilon_{\mathbf{k}}$ for the band energy at crystal momentum $\mathbf{k}$, e for the elementary charge, $\mathbf{E}$ and $\mathbf{B}$ for electric and magnetic field, respectively, while, crucially, the first cross product term represents a correction due to the Berry curvature $\mathbf{\Omega}_{\mathbf{k}}$ and a driving force $\dot{\mathbf{k}}$. Such a modification applies even outside of electron systems. For example, a Hall effect of light was proposed, where an electromagnetic wave packet scatters at an interface between two optically different media [20, 21]. While geometric ray optics may properly describe the macroscopic classical behavior, a proper derivation and analysis of the electromagnetic equations of motion using optical wave packets revealed Berry curvature corrections that laterally shift the reflected and the transmitted light rays at the interface.

In the present paper we study the transport dynamics of semiclassical electrons in graphene in the Klein tunneling regime by scattering wave packets off a potential step while taking the full graphene Hamiltonian into account. Our main findings are two-fold. First, our numerical simulation reveals in some cases unusual side shifts and/or kinks in the wave packet motion near the step edge. These features indicate deviations from a simple reflection law or Snell's law and are reminiscent of the optical Hall effect, suggesting the presence of a Berry curvature velocity where the driving force is the potential gradient at the step edge [see Eq. (1)]. This can be seen in Fig. 1 (a), which shows the trajectories of three wave packets propagating towards a potential step. Each wave packet splits into a transmitted and a reflected part upon striking the potential step, which is much taller than the wave packets' energies (i.e., the setup represents a pn junction). Looking at the red pair of trajectories (full circles), the path of the wave packet fraction in region I, which denotes the lower part of the step at zero potential height, clearly exhibits a shift roughly parallel to the step edge. A shift or kink in the wave packet motion can also occur on the transmission side, which is marked as region II and forms the upper part of the step. Second, we establish the basic transmission characteristics that, in contrast to usual Klein paradox studies involving graphene, include intervalley coupling, finite bandwidth effects and band anisotropy effects. Our results in particular reveal striking differences in the Klein tunneling behavior at zigzag and armchair steps. All in all, the

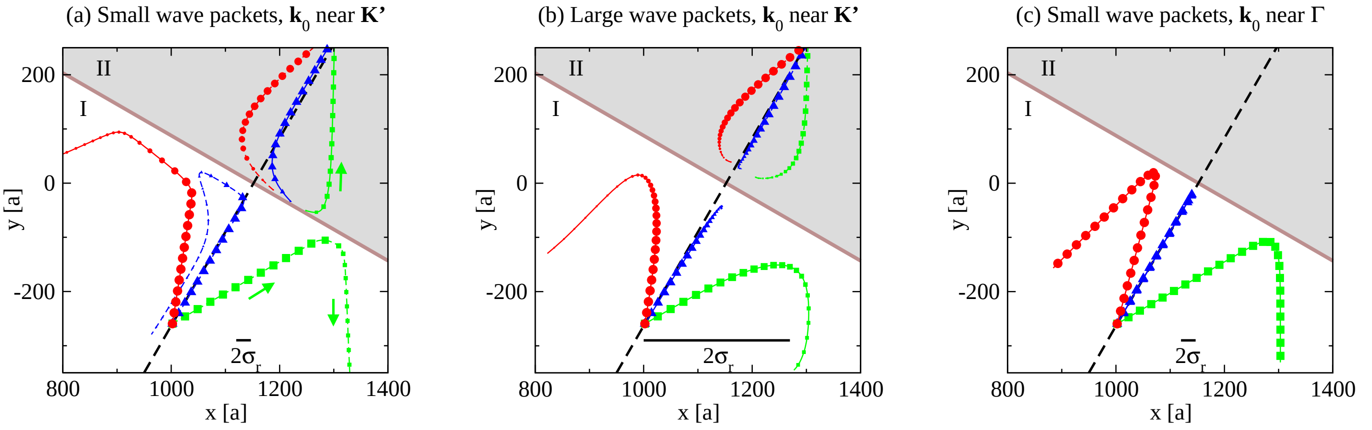

FIG. 1. (Color online) Trajectories of wave packets scattering at a zigzag potential step roughly twice taller than their incoming kinetic energies. The zigzag step edge is marked by the solid brown line, separating the lower part of the step (region I, white) from the upper part (region I, grey), while the dashed black line lies normal to the step edge and serves as a guide to the eye. The size of the symbols along the trajectories stand for the probability weights $P_{\mathrm{I/II}}(\tau)$, while the black line at the bottom indicates the initial wave packet diameter ($2\sigma_r$). In (a) small wave packets with $\mathbf{k}_0$ near $\mathbf{K}'$ break up into a reflected (region I) and a transmitted fraction (region II) upon approaching the step edge (the green arrows representatively illustrate the scattering process). Remarkably, the set of trajectories appears completely asymmetric with respect to the step normal, while the red (full circles) and the blue (full triangles) trajectories feature unusual lateral shifts and/or kinks close to the step edge. These features gradually disappear (b) with increasing wave packet size or (c) by moving $\mathbf{k}_0$ closer to the Γ point. Note that the bending of the green trajectory (full squares) near the x-axis in panel (b) is a finite size effect. Please see main text and [29] for details.

dynamics near the step edge sensitively depend on the wave packet and the step potential parameters and will be discussed in more detail below.

Semiclassical wave packet propagation — To study the single electron dynamics we consider a spinless electron wave packet moving in a two-dimensional honeycomb lattice towards a sharp potential step. Although it is experimentally challenging to fabricate graphene devices with thin junction interfaces, a sharp potential step is the simplest setup and an instructive limit to investigate semiclassical Klein tunneling.

The time evolution of the wave packet $|\psi(\tau)\rangle$ is governed by the time-dependent Schroedinger equation $i\partial_\tau|\psi(\tau)\rangle = (H_0 + H_{\mathrm{step}})|\psi(\tau)\rangle$, which contains the usual honeycomb tight-binding Hamiltonian H_0 with nearest-neighbor hopping t [1] and a step potential

$$H_{\mathrm{step}} = \sum_{\mathbf{r}} [V(\mathbf{r}) a^\dagger_{\mathbf{r}} a_{\mathbf{r}} + V(\mathbf{r}+\vec{\delta}) b^\dagger_{\mathbf{r}} b_{\mathbf{r}}], \tag{2}$$

characterized by step height V_0 (i.e. $V(\mathbf{r}) = 0$ (V_0) for $\mathbf{r} \in$ I (II)). Here $a^\dagger_{\mathbf{r}}$ ($b^\dagger_{\mathbf{r}}$) creates an electron on sublattice A (B) in unit cell $\mathbf{r}$, while $\vec{\delta}$ denotes the intra-unit cell nearest-neighbor vector. Below we express all distances in units of the nearest-neighbor distance a, momenta in units of $1/a$ and energies in units of t.

The wave packet evolution then follows straightforwardly from a fourth order split-operator (Suzuki-Trotter) approximation scheme $|\psi(\tau)\rangle \approx \Pi_{n=1}^{N} \mathrm{e}^{-iH\Delta\tau}|\psi(\tau=0)\rangle$, where $\Delta\tau = \tau/N$ and N is the total number of iterations [22, 23]. For simplicity, we impose periodic boundary conditions and use sufficiently large system sizes and small enough time steps to reduce finite size effects.

The wave packet evolution in graphene depends sensitively on the initial wave packet setup. Although we evolve the wave packet numerically using the real space representation, i.e.

$$|\psi(\tau)\rangle = \sum_{\mathbf{r}} [\Psi_A(\mathbf{r};\tau) a^\dagger_{\mathbf{r}} + \Psi_B(\mathbf{r};\tau) b^\dagger_{\mathbf{r}}]|0\rangle, \tag{3}$$

where $\Psi_{A(B)}(\mathbf{r};\tau)$ stands for the wave function on sublattice A (B), it is convenient to specify the initial wave packet at $\tau = 0$ using the eigenbasis of the H_0. Thus in the following, if not stated otherwise, the initial wave packet is given as a Gaussian-like superposition of positive energy eigenstates centered close to the K' point

$$|\psi(\tau=0)\rangle = \sum_{\mathbf{k}} \Psi_{\mathbf{k}_0,\sigma_k,\mathbf{r}_0}(\mathbf{k}) \xi^\dagger_{\mathbf{k}} |0\rangle, \tag{4}$$

where $\xi^\dagger_{\mathbf{k}}$ creates a state with momentum $\mathbf{k}$ in the electron band [24]. The momentum distribution $\Psi_{\mathbf{k}_0,\sigma_k,\mathbf{r}_0}(\mathbf{k})$ is centered at $\mathbf{k}_0$ and characterized by a width σ_{k}, while the position in real space is given by $\mathbf{r}_0$. Initializing the wave packet using states from both electron and hole bands would complicate the propagation dynamics as additional interference phenomena such as trembling motion (*Zitterbewegung*) may appear [25–28].

Possible Berry curvature effect — Let us investigate the wave packet dynamics in graphene in more detail.

Panel (a) in Fig. 1 shows three sets of wave packet trajectories where the incoming wave packets emanate from the same point in region I, but have different central momenta $\mathbf{k}_0$ located close to the K' point (for precise momentum values see [29]). These wave packets have similar total energies ($\epsilon_0 \approx 0.4t > 0$) and sizes (set by the spread in momentum space $\sigma_k = 0.2/a$, which corresponds to a real space standard deviation of $\sigma_r \approx 13.48a$), but strike the zigzag step edge at different angles. At the step edge ($V_0 = 0.8t$) the incoming wave packets are partially reflected and partially transmitted. To follow the reflection and transmission dynamics, the trajectories in region I and II are defined via the centre of mass motion of the wave packet fractions. The total probability weight of each fraction is given by

$$P_{\mathrm{I}}(\tau) = \sum_{\mathbf{r}\in I} |\Psi_A(\mathbf{r};\tau)|^2 + \sum_{\mathbf{r}+\vec{\delta}_1\in I} |\Psi_B(\mathbf{r};\tau)|^2 \qquad (5)$$

and $P_{\mathrm{II}}(\tau) = 1 - P_{\mathrm{I}}(\tau)$, respectively, and indicated by the size of the full symbols accompanying the trajectories.

To extract the semiclassical dynamics, panel (b) shows the evolution of large wave packets ($\sigma_k = 0.02/a$, $\sigma_r \approx 134.8a$) with similar momenta and energies as in (a), while panel (c) displays the propagation of small wave packets ($\sigma_k = 0.2/a$) as in (a), which, however, are initially composed of hole states with momenta near the Γ point instead of the K' point. Here, the wave packets' initial kinetic energy and the step height measured from the bottom of the hole band are $\epsilon_0 \approx 0.2t$ and $V_0 = 0.4t$, respectively. All wave packet and step setups in Fig. 1 correspond to a pn junction ($0 < \epsilon_0 < V_0$). Please see also the supplemental material for animations corresponding to the red (full circles) wave packet trajectories in (a)-(c).

There are several interesting features associated with the wave packet motion. Obviously, reflection and transmission of small wave packets do not simply follow a reflection law ($\theta_{\mathrm{in}} = \theta_{\mathrm{refl}}$) or a variation of Snell's law ($n_{\mathrm{in}}\sin\theta_{\mathrm{in}} = n_{\mathrm{trans}}\sin\theta_{\mathrm{trans}}$), respectively. As noted before, the wave packet portion in region I near the step edge experiences in some cases a side shift roughly parallel to the edge and/or abrupt changes in the propagation direction. On the transmission side (region II), the trajectories can also exhibit unusual features (side shifts and kinks) close to the step edge, depending on the incoming wave packet direction and the step height, and can vary strongly in orientation and the transmitted probability weight. This is shown in the supplemental material, where similar simulation results (including lateral shifts and offsets) for other step configurations such as pp junctions ($0 < V_0 < \epsilon_0$) and armchair step edges are presented. Considering all trajectories together, the scattering process in Fig. 1 moreover appears strikingly asymmetric with respect to the step normal, which is characteristic of the zigzag edge and in stark contrast to the highly symmetric trajectories appearing at an armchair edge.

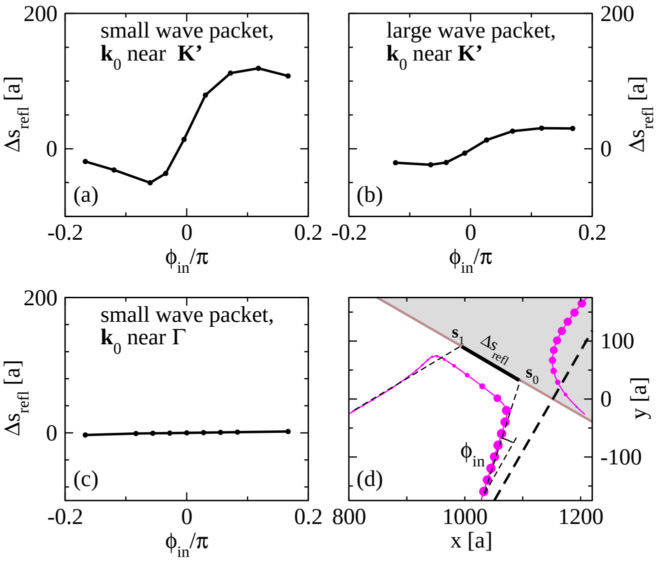

FIG. 2. (Color online) Side shifts [panels (a)-(c)] for the three different step scenarios presented in Fig. 1. Panel (d) illustrates the definition used here for the lateral shift Δs and the incoming angle ϕ_{in}. A substantial lateral shift occurs only for small wave packets with initial momenta near $\mathbf{K}'$, supporting the notion of a Berry phase effect. Please see main text for details.

One can attempt to quantify the overall lateral shifts by measuring the difference between the intersections of the asymptotes of the incoming and the reflected wave packet paths in region I with the step edge. The separation of the intersections $\Delta s = |\mathbf{s}_1 - \mathbf{s}_0|$ as a function of the incoming angle ϕ_{in} is plotted in Fig. 2. This way of characterizing the side shift works best for wave packet paths close to the step normal where changes in the propagation direction are rather abrupt and unaffected by finite size effects, which tend to occur for larger incoming angles and larger wave packets.

Figures 2 (a), (b) indicate a drastic difference between small and large wave packet dynamics. With increasing wave packet size the side shifts gradually disappear. By analogy to the Hall effect of light, the trajectory anomalies therefore may arise from a Berry curvature velocity [see Eq. (1)], which is known to modify the semiclassical equations of motion of Bloch electrons in systems with broken inversion or time-reversal symmetry [18, 19]. A Berry curvature term can only be effective for a finite distribution of wave vectors and hence may be diminished or absent in the limit of very large wave packets and plane wave states.

Since Berry curvature effects are usually strongest near the Dirac points, one can further check the dynamics of small wave packets that are initially composed of hole states near the Γ point as shown in Fig. 1 (c). Such

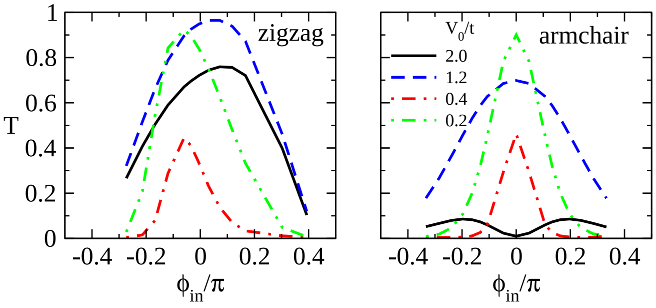

FIG. 3. (Color online) Transmission profiles for zigzag and armchair step edges with various step heights V_0 as a function of incoming angle $\phi_{\rm in}$ [see also Fig. 2 (d)]. All wave packet energies and sizes are fixed at $\epsilon_0 \approx 0.4t$ and $\sigma_k = 0.2/a$ (small wave packets), respectively, as in Fig. 1 (a). We note that with increasing step height, the finite bandwidth of the graphene dispersion suppresses the transmission probability T (see black curves).

wave packets resemble quantum particles in an ordinary parabolic band and undergo a total reflection at tall potential steps and are partially transmitted and reflected at sufficiently low potential steps. Transverse shifts or kinks in the trajectories are completely absent [see also Fig. 2 (c)], which is consistent with a vanishing Berry curvature near the Γ point. Given these observations, one may therefore speculate that the magnitude of the side shift is roughly determined by the Berry curvature flux through the footprint of the wave packet distribution in momentum space (or by the difference thereof between the initial and the final states).

Finally, we briefly comment on the role of edges states, which have a topological origin [30, 31]. Edge states play only a minor role since the trajectory anomalies are associated with both the zigzag and the armchair edge (see supplemental material). Furthermore, the zigzag edge states are located energetically just above ($\gtrsim V_0$) and just below the step ($\lesssim 0$) and thus are energetically far removed for the cases considered here. It may be interesting though to consider situations where the zero mode edge states are relevant.

Basic transmission characteristics — Let us now focus on the basic Klein tunneling transmission characteristics in graphene. The easiest way to distinguish a zigzag from an armchair step is by analyzing the transmission profiles. Approximating the transmission probability $T = P_{\rm II}(\tau \to \infty)$ by the probability weight in region II at the largest simulation time available, differences in the scattering dynamics are clearly visible in Fig. 3. Although the transmission curves in both cases are strongly angle dependent, the armchair curves are highly symmetric about $\phi_0 = 0$, while the zigzag counterparts are not. Another striking feature revealed in Fig. 3 is that the transmission probability is substantially suppressed for tall step heights ($\epsilon_0 \ll V_0$), see e.g., the solid black ($V_0 = 2.0t$) and the dashed blue curves ($V_0 = 1.2t$). This is in contrast to the usual Klein paradox of relativistic Dirac fermions, where transmission over a wide angle range approaches unity with increasing step height. The non-monotonous behavior of the transmission curves at $V_0 = \epsilon_0$, however, remains preserved (see dashed blue, dash-dotted red, and dash-double-dotted green curves) [14–17].

Both the symmetry difference between zigzag and armchair step edges and the decreased wave packet transmission for tall steps result from taking naturally the full graphene dispersion into account in the numerical simulation. The graphene band structure exhibits a trigonal symmetry away from the Dirac points and possesses a finite bandwidth. The latter leads to the reduced transmission probability for large potential steps due to the lack of appropriate scattering states on the high step side. The band anisotropy, on the other hand, directly affects the reflection and transmission trajectories further away from the step edge and hence is encoded in the transmission profiles. For example, a zigzag edge involves only intra-valley scattering. The dominant reflection and transmission states in the present study therefore are limited via energy conservation and momentum conservation parallel to the edge direction to states around the K' point, which, depending on the step height, can even give rise to a preferred overall transmission direction (not shown). In contrast, an armchair step potential connects the two inequivalent Dirac points, which are related by inversion and time-reversal symmetry and thus produces more symmetric wave packet motion as a function of incoming angle.

Conclusion — We have investigated the Klein tunneling of electrons at zigzag and armchair step potentials employing the full graphene Hamiltonian and a semiclassical wave packet approach. Apart from establishing distinct transmission characteristics for zigzag and armchair steps, we have identified unusual wave packet dynamics near the step edge. These unusual features appear for both zigzag and armchair step orientations and support the notion of Berry curvature influenced semiclassical Klein tunneling. These anomalies may help resolve the discrepancy found in the angle dependence of Klein tunneling reported in [10]. Further extension of the numerical simulations may include a magnetic field, smooth potential steps, which may lead to mixing with Bloch oscillation phenomena, and potential barriers, which are useful for electron focussing and lensing in graphene [32].

The authors thank T. Nakanishi, K. Wakabayashi and N. Kumada for useful discussions. Y. H. acknowledges partial financial support through Grants-in-Aid (KAKENHI No. 23340112 and No. 23654128) from JSPS.

---

* cpuetter@comas.frsc.tsukuba.ac.jp

[1] A. H. Castro Neto, F. Guinea, N. M. R. Peres, K. S. Novoselov and A. K. Geim, Rev. Mod. Phys. **81**, 109 (2009).

[2] K. S. Novosolov, A. K. Geim, S. V. Morozov, D. Jiang, M. I. Katsnelson, I. V. Griegorieva, S. V. Dubonos, and A. A. Firsov, Nature **438**, 197 (2005).

[3] Y. Zhang, Y.-W. Tan, H. L. Stormer, and P. Kim, Nature **438**, 201 (2005).

[4] Y. Hatsugai, T. Fukui, and H. Aoki, Phys. Rev. B **74**, 205414 (2006).

[5] N. Nagaosa, J. Sinova, S. Onoda, A. H. MacDonald, and N. P. Ong, Rev. Mod. Phys. **80**, 1083 (2010).

[6] O. Klein, Z. Phys. **53**, 157 (1929).

[7] J. R. Williams, L. DiCarlo, and C. M. Marcus, Science **317**, 638 (2007).

[8] B. Huard, J. A. Sulpizio, N. Stander, K. Todd, B. Yang, and D. Goldhaber-Gordon, Phys. Rev. Lett **98**, 236803 (2007).

[9] R. V. Gorbachev, A. S. Mayorov, A. K. Savchenko, D. W. Horsell, and F. Guinea, Nano Lett. **8**, 1995 (2008).

[10] N. Stander, B. Huard, and D. Goldhaber-Gordon, Phys. Rev. Lett **102**, 026807 (2009).

[11] A. F. Young, and P. Kim, Nat. Phys. **5**, 222 (2009).

[12] R. N. Sajjad, N. Sutar, J. U. Lee, and A. W. Gosh, arXiv:1207.6619 (2012).

[13] K. J. A. Reijnders, T. Tudorovskiy, and M. I. Katsnelson, arXiv:1206.2869 (2012).

[14] M. I. Katsnelson, K. S. Novoselov, and A. K. Geim, Nat. Phys. **2**, 620 (2006).

[15] V. V. Cheianov and V. I. Fal'ko, Phys. Rev. B **74**, 041403 (2006).

[16] N. M. R. Peres, J. Phys.: Condens. Matter **21**, 323201 (2009).

[17] P. E. Allain and J. N. Fuchs, Eur. Phys. J. B **83**, 301 (2011).

[18] D. Xiao, M.-C. Chang, and Q. Niu, Rev. Mod. Phys. **82**, 1959 (2010), and references therein.

[19] M.-C. Chang and Q. Niu, J. Phys.: Condens. Matter **20**,193202 (2008), and references therein.

[20] M. Onoda, S. Murakami, and N. Nagaosa, Phys. Rev. Lett. **93**, 083901 (2004).

[21] M. Onoda, S. Murakami, and N. Nagaosa, Phys. Rev. E **74**, 066610 (2006).

[22] M. Suzuki, Phys. Lett. A **146**, 319 (1990).

[23] M. Suzuki, J. Phys. Soc. Jpn. **61**, 3015 (1992).

[24] For numerical reasons we actually use a Cosine distribution instead of a Gaussian, which is a close approximation.

[25] M. I. Katsnelson, Eur. Phys. J. B **57**, 225 (2007).

[26] T. M. Rusin and W. Zawadzki, Phys. Rev. B **76**, 195439 (2007).

[27] G. M. Maksimova, V. Ya. Demikhovskii, and E. V. Frolova, Phys. Rev. B **78**, 235321 (2008).

[28] J. Cserti and G. David, Phys. Rev. B **82**, 201405 (2010).

[29] The Dirac points are located at $\mathbf{K} = (K_x, K_y) = 2\pi/3a(1, 1/\sqrt{3})$ and $\mathbf{K}' = (K_x, -K_y)$. In panel (a) and (b) of Fig. 1, the initial central momenta are $\mathbf{k}_0 = -0.895(K_x, K_y)$, $(-0.954K_x, -0.782K_y)$, and $(-0.988K_x, -0.761K_y)$ for the red (circles), blue (triangles), and green (squares) trajectories, respectively. In (c) the momenta are $\mathbf{k}_0 = 0.216(K_x, K_y)$, $(0.125K_x, 0.374K_y)$, and $(0.065K_x, 0.417K_y)$ for the same trajectory order.

[30] M. Fujita, K. Wakabayashi, K. Nakada, and K. Kusakabe, J. Phys. Soc. Jpn. **65**, 1920 (1996).

[31] S. Ryu and Y. Hatsugai, Phys. Rev. Lett. **89**, 077002 (2002).

[32] V. V. Cheianov, V. I. Fal'kov, and B. L. Altshuler, Science **315**, 1253 (2007).

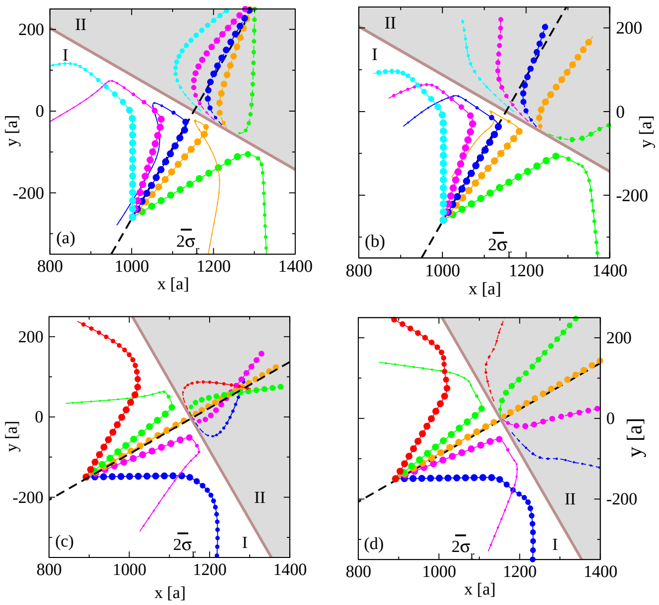

FIG. 4. (Color online) Wave packet trajectories complementary to those in Fig. 1 of the main text. The wave packets' incoming kinetic energies are roughly $\epsilon_0 \approx 0.4t$ and their sizes are given by $\sigma_k = 0.2/a$ ($\sigma_r \approx 13.48a$) as in Fig. 1 (a). In the two upper panels, the step orientation is parallel to the zigzag direction. Panel (a) contains more trajectories, but is otherwise the same as Fig. 1 (a), where the step height amounts to $V_0 = 0.8t$ (pn junction). In panel (b) the potential jump is smaller than the wave packet energy $V_0 = 0.2t < \epsilon_0$ (nn junction), representing the classical transmission regime. Panels (c) and (d) are the armchair counterparts of (a) and (b), respectively.

SUPPLEMENTAL MATERIAL

Wave packet animations — A set of movies corresponding to the red (full circles) wave packet trajectories in Fig. 1 is available at `youtube`.

Armchair steps and more — Figure 4 shows a selection of wave packet trajectories for different step configurations. The step setup in panel (a) is identical to that of Fig. 1 (a), but here were present a wider selection of wave packet trajectories with varying incoming angles. The overall shift of the reflected trajectories is clearly noticeable. In contrast to (a), panel (b) shows the trajectories of the same initial wave packets scattering at a lower step ($\epsilon_0 > V_0$). In this case, there are not only lateral shifts of the reflected wave packet fractions, but also overall lateral offsets of the transmission trajectories with respect to the incoming direction for larger ϕ_{in}, see e.g. the cyan colored trajectories (leftmost trajectory pair) in (b). Unusual features in the wave packet motion also occur at armchair steps as displayed in panels (c) and (d) for high and low step potentials, respectively. The armchair case therefore produces not only trajectories that are highly symmetric about the step normal, but also unusual due to overall lateral shifts and offsets.